Chapter 4

Development of trans-ribozymes as actuators controlling gene expression

Abstract

The modular and tunable nature of RNA makes it ideal to perform both sensing and actuation functions within an synthetic control system [1]. RNA regulates gene expression through a variety of mechanisms at the transcriptional, post-transcriptional, and translational levels. Ribozymes are RNA molecules that regulate gene expression through post-transcriptional cleavage of target RNA. While their ability to cleave transcripts in a sequence-specific manner makes trans-ribozymes attractive candidates for targeting therapeutically relevant transcripts, applications have been limited by poor *in vivo* efficiency. However, through the recent elucidation of the design rules for *in vivo* catalytic activity, hammerhead ribozymes are now poised to be effective regulators of gene expression. In this work, we apply the rules for *in vivo* activity established for cis-ribozymes to the development of more effective trans-ribozymes. We demonstrate that precise engineering of the intramolecular reaction between the ribozyme and target transcript is required for efficient cleavage at physiological Mg^{2+} concentrations. To improve the correlation between our *in vitro* and *in vivo* assays of ribozyme cleavage efficiency, we employed a dual cis-hammerhead ribozyme cassette to excise our trans-ribozyme designs from the ribonucleoprotein (RNP) *in vivo*. Finally, we varied the levels of target sequence to examine how the concentration of target transcript, and consequently, the ratio of ribozyme to target affect target knockdown levels. These experiments demonstrated that knockdown efficiency has a biphasic relationship to target transcript levels. Our results suggest that one of the key limitations to trans-ribozyme-mediated knockdown may be facilitating the intermolecular binding event between the trans-acting ribozymes and the target transcript. While this limits the potential application

space of trans-acting ribozymes, it may position these devices as uniquely targeted regulators of endogenous transcripts associated with cell proliferation whose expression must be precisely balanced to maintain normal cellular growth while preventing serious pathologies that result from overexpression. Finally, trans-ribozymes maybe aptly suited to regulating expression within synthetic gene networks where transcript colocalization can be mediated via expression of the trans-ribozyme and target transcript from the same vector.

Introduction

Novel cellular behaviors can be generated by coupling engineered control systems to the cell's natural regulatory network [2]. However, the ability to run preprogrammed control algorithms depends on the facile construction of modular input / output interfaces between endogenous and synthetic systems. Currently, engineering gene circuits relies heavily on engineering protein-DNA interactions to control transcription. The rational design of protein-based control systems has been impeded by our limited understanding of how to engineer precise tertiary structures into proteins. Until it is possible to efficiently construct *de novo* connections between native and synthetic circuitry, the application of cellular programming strategies will be limited to a small set of input and output interfaces. As a result of these limitations, widespread application of exogenous control to cellular engineering applications remains unfeasible.

The modular and tunable nature of RNA makes it an ideal candidate to perform both sensing and actuation functions within an exogenous control system**.** Already researchers have demonstrated that RNA is capable of targeted gene knockdown through RNAi, trans-acting ribozymes, and antisense mechanisms [3-5]. However, the current technologies are limited in their ability to be integrated into robust, modular control systems. Off-target effects and poor efficiency hinder the effective application of antisense regulation of gene expression [5]. Hijacking the RNAi pathway has raised concerns that saturating the cellular machinery with heterologous substrates competes with the processing of endogenous RNAi substrates and can result in off-target or other undesired effects [6]. Additionally, RNAi is not universal throughout eukaryotic organisms such as *Saccharomyces cerevisiae*, a model organism for studying the

activation of various cancer pathways [7-9]. Ribozymes may offer an alternative gene regulatory mechanism upon which to build flexible, modular control systems.

Ribozymes are RNA molecules that catalyze a variety of chemical reactions such as self-cleavage or ligation [10]. The hammerhead ribozyme is comprised of three helical regions that converge on a highly conserved catalytic core of eleven nucleotides (nts) (Figure 4.1A) [11]. Cleavage is sequence-specific and targets a 5'-NUX-3' triplet, where N is any base, U is uracil, and X is any base except guanine. The optimal NUX for efficient and fast cleavage is GUC. Ribozyme cleavage is catalyzed when the 2' hydroxyl group from X directly 3' of the cleavage site is deprotonated. This nucleophile then attacks the scissile phosphate and, through a penta-coordinated trigonal bi-pyramidal transition state, produces a 5' and 3' product (Figure 4.1B) [12].
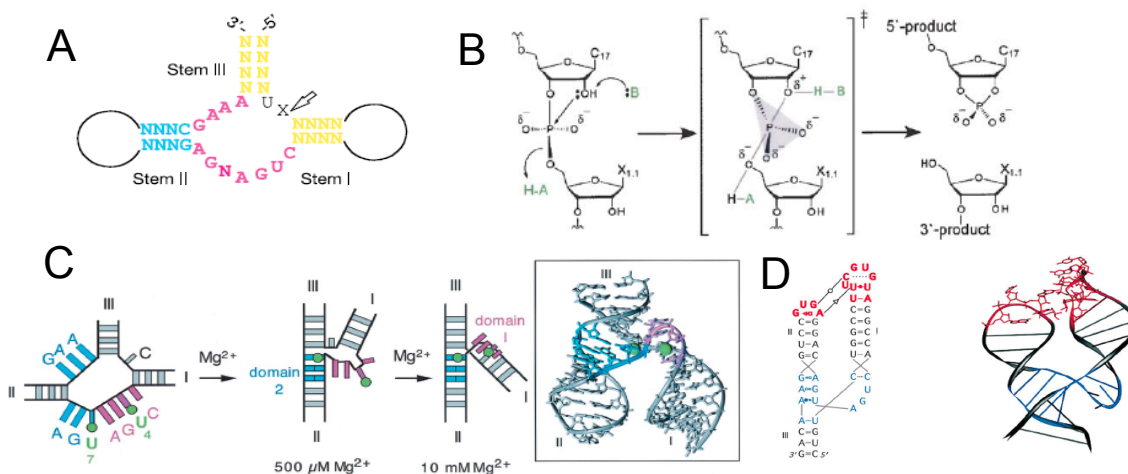

Figure 4.1. The hammerhead ribozyme. A) The catalytic core is shown in pink with the NUX sequence in black. The flanking helical regions are shown in yellow. Stem II is shown in blue. Black circles represent stem loops. Figure adapted from [13]. B) Ribozyme cleavage mechanism at the NUX triplet. Figure adapted from [12]. C) Folding of the ribozyme is thought to proceed through two magnesium binding events. Figure adapted from [14]. D) The "Y"-shaped ribozyme is thought to be stabilized by loop interactions between unpaired bases in the stem loops. Figure adapted from [11].

Folding of the ribozymes into an active conformation is postulated to proceed through dual divalent ion binding events (Figure 4.1C). A high affinity binding event occurs at 500 μM and orders the first set of tertiary interactions. The second low affinity addition of ion occurs at 10 mM and restructures the ribozyme stem orientations such that helix I folds away from helix III and interacts with helix II [14]. Ribozymes with a conserved catalytic core that do not maintain specific helical regions are called minimal ribozymes (mRzs). While at high divalent ion concentrations (10 mM) mRzs are active, at lower concentrations mRzs are effectively inert [11, 15]. Crystal structures of natural ribozymes depict a "Y"-shaped molecule that has two of the helical regions interacting as "kissing loops" (Figure 4.1D) [16]. Given the "kissing loop" interaction between the two helical regions, tertiary interactions between unpaired bases in the stem loops are proposed to stabilize the catalytically active conformation and obviate high divalent ion conditions. Researchers have demonstrated restored *in vitro* catalytic activity at biologically relevant divalent ion concentrations, between 100 and 300 μM, by reincorporating the loops into minimal ribozyme designs [11, 15, 17-20].

While the list of naturally occurring ribozymes is limited to cis-acting elements that perform intramolecular cleavage, synthetic trans-acting hammerhead ribozymes (thRzs) have been demonstrated that cleave intermolecular target sequences [4, 21, 22]. With their potential ability to target endogenously expressed transcripts, thRzs offer a significant advantage over their cis-acting counterparts, chRZs (Figure 4.2). Further, unlike cis regulatory elements, trans-acting elements like thRzs allow decoupling of ribozyme and target expression levels, offering the potential to tune knockdown via the independent modulation of thRz levels. While *in vitro* cleavage assays confirm that

trans-ribozymes cleave target transcripts specifically [23, 24], *in vivo* demonstrations of targeted gene regulation with trans-ribozymes are limited and restricted to higher eukaryotes [22, 25]. In addition, *in vivo* knockdown of gene expression remains hampered by low trans-ribozyme activity in the intracellular environment [20]. However, *in vivo* design rules have recently been specified and applied toward the construction of ribozymes that effectively regulate gene expression in cis through self-cleavage when placed in the 3' untranslated region (UTR) of target transcripts [26]. The application of the *in vivo* design rules that have been successfully implemented to convert cis-ribozymes into effective regulators of gene expression may be applied to trans-ribozymes to increase their efficacy as gene regulatory elements. Finally, while the simple knockdown of target genes is scientifically and clinically important, conditional regulation of gene products through integrated molecular control systems offers the potential to temporally and spatially tune therapies to restore proper function in diseased cells. Designing robust RNA-based control systems necessitates well-defined, modular actuators. By delineating the requirements for *in vitro* and *in vivo* activity we intend to examine the plasticity of the ribozyme domains requisite for targeting novel endogenous transcripts. Further, given the rules for constructing ligand-responsive chRz switches have recently been established [26], we evaluate the potential for constructing ligand-responsive RNA switches from the trans-acting ribozyme platform.

A

B

C
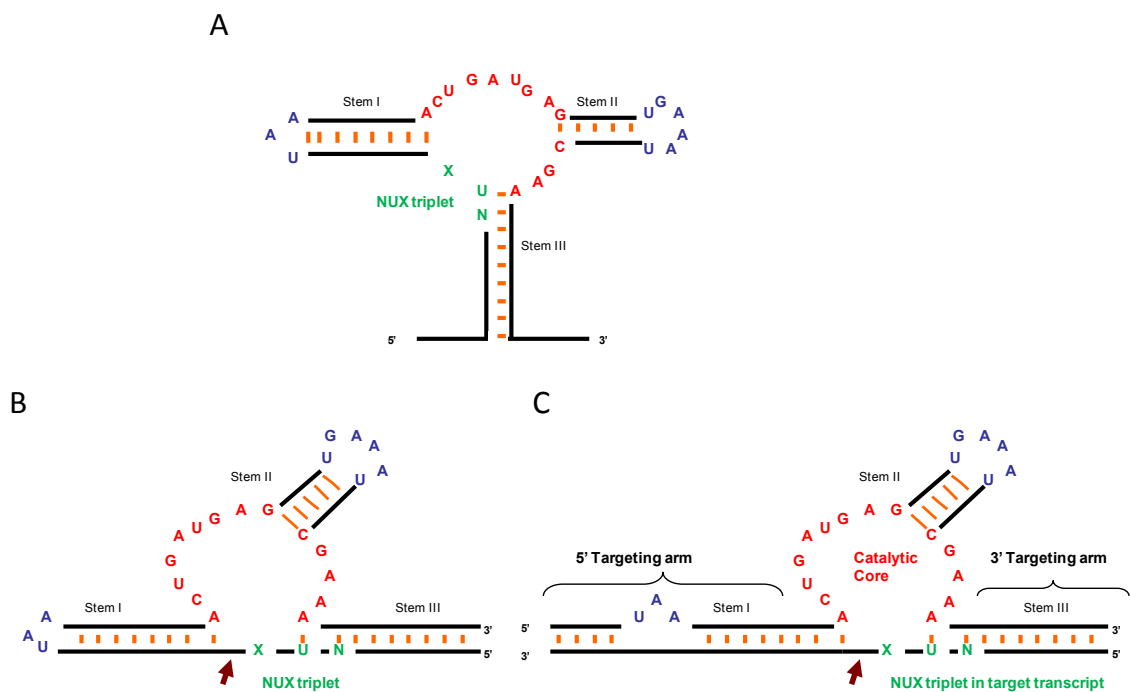
Figure 4.2. The anatomy of a cis-acting hammerhead ribozyme and trans-acting hammerhead ribozyme with target transcript. A. Canonical representation of cis-acting hammerhead ribozyme (chRz) with PLMVd loops incorporated into transcript via stem III. Stem I and stem II branch off catalytic core to give the eponymous hammerhead shape. **B.** A cis-acting hammerhead ribozyme with stem III rotated counter-clockwise 90° with stem I fixed for simple comparison with trans-acting counterpart. **C.** Trans-acting hammerhead ribozyme (thRz) hybridized with target transcript. For all representations the catalytic core is shown in red and NUX triplet shown in green. Converting cis-acting ribozymes to trans-acting opens stem I from a closed loop. Preserving the loop (shown in blue) from the chRz require these nucleotides to be unpaired as a bulge. At low Mg^{+2} concentrations, the bulge in stem I and stem loop II (shown in blue), interact to stabilize the active conformation (Figure 1D). These interactions are found in natural chRzs and have been adapted for engineered thRzs.

In this work, we have taken the rules established for effective *in vivo* activity of chRzs and applied them to the development of thRzs. We demonstrate additional design constraints for efficient thRz cleavage in engineering the intramolecular binding event between the ribozyme and target transcript. In particular, we demonstrate that engineering the stem loops and the length of the targeting arms of the thRz is necessary to achieve efficient cleavage of the target transcript *in vitro*. Finally, we observe that thRz knockdown varies biphasically with target expression levels. Taken together these data

suggest that thRz knockdown is highly context-dependent and limited by system constraints that govern the intermolecular binding event.

Results

Initial thRz designs demonstrate *in vivo* limitations

The initial thRz designs were adapted from previous *in vitro* studies [20] to target a region in the transcript encoding yEGFP (yeast enhanced green fluorescent protein). We focused on developing thRzs that specifically target a fluorescent reporter protein (yEGFP) as an initial design goal as it allows us to quantify gene knockdown activity through fluorescence-based assays. In addition, yEGFP can be used to monitor various endogenous proteins via protein fusions, such that a trans-acting yEGFP ribozyme can be directly applied to regulate the expression of any coding sequence tagged with the target sequence from the yEGFP fluorescent protein. While the plasticity of the targeting arms is yet to be fully explored, we anticipate that the targeting arms will prove to be amenable to targeting a variety of sequences. Therefore, by modifying the targeting arms of the developed thRz construct we expect that we can adapt the system to target a wide array of cellular transcript.

The initial trans-ribozyme designs conformed to the following composition rules. First, the catalytic core was conserved to maintain activity (Figure 4.2C). Second, the target transcript contains a NUX triplet, where N is any base, U is uracil, and X is any base but guanine. Finally, for *in vivo* activity, the catalytically active "Y" shaped conformation must be formed. To achieve this requirement at physiological Mg^{2+} concentrations, the nucleotides in the bulges in stem I and stem II, are designed to

interact to stabilize the active conformation. These stem loop sequences are derived from those found in the peach latent mosaic viroid (PLMVd) ribozyme, a natural chRz [11]. Adopting these loops requires careful design considerations when selecting a target sequence. The bulge region must maintain unpaired nucleotides such that the targeted region in the target transcript does not have sequence complementarity to this region of the thRz. Additionally, canonical PLMVd ribozymes exhibit particular stem lengths between the stem I loop, the stem II loop, and the catalytic core, which were maintained in our designs. In stem I, 5 base pairs separate the bulge sequence from the catalytic core. In stem II, 4 base pairs separate the catalytic core and the stem loop sequence. Thus, canonical ribozymes will adopt the following nomenclature "X54" where X denotes the number of base pairs formed between the targeting arm sequence and the transcript 5' of the bulge (Figure 4.3).
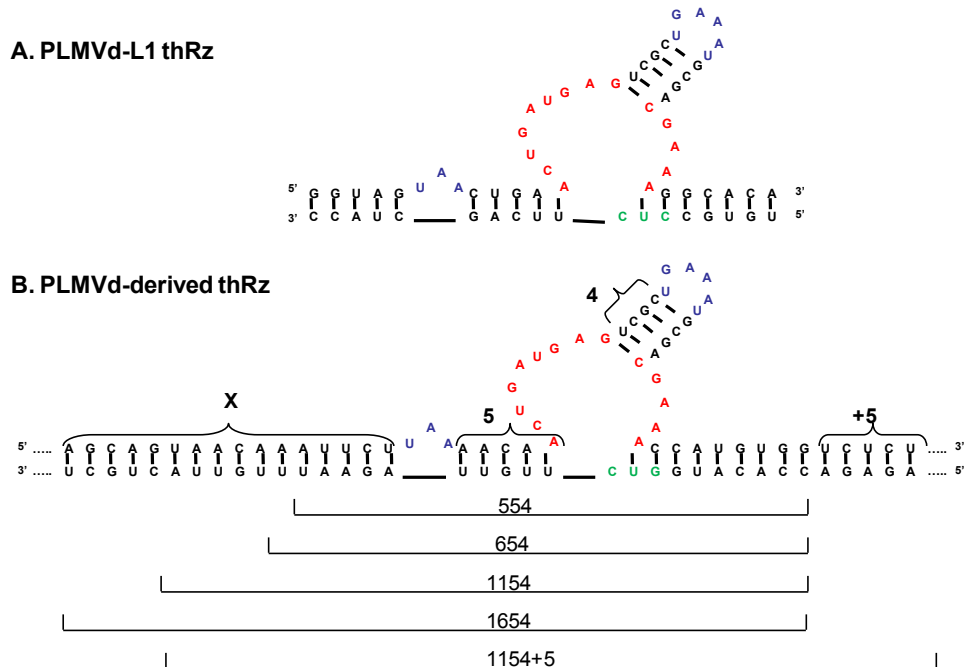
Figure 4.3. Various thRz designs. A. Previous *in vitro* studies focused on incorporating the PLMVd-derived stem loops into thRz targeted a segment of HIV1 mRNA, PLMVd-L1 thRz adapted from [20]. **B.** By redesigning the targeting arms, we created a series of PLMVd-derived thRzs targeting a sequence in yEGFP.

The initial thRz designs were characterized through *in vitro* cleavage assays in which separately transcribed ribozymes and radiolabeled target sequences were purified, combined, annealed, and incubated. Annealing was performed to allow transcripts to escape nonminimal free-energy structures potentially adopted during column purification. Endpoint cleavage efficiency was determined by comparing the amount of full-length to cleaved target sequence when visualized via PAGE gel and phosphorimaging analysis (see Methods). We modified our cleavage assay from previously reported methods to facilitate a more accurate correlation between *in vitro* results and *in vivo* activity. Specifically, we extended the length of the target transcript beyond the region that binds to the targeting arms. By including the peripheral transcript regions, we were attempting to more closely recapitulate the folding microenvironment of the full-length transcript for the region of interest. For example, the flanking sequences might interact with the target region to form secondary structures that might impede hybridization of the trans-ribozyme to the target region and thus cleavage. Accessibility of the target sequence is known to control the efficacy of thRz knockdown *in vivo* [27]. By targeting a RNA strand that more closely resembles *in vivo* transcripts, the *in vitro* cleavage assays are expected to reflect *in vivo* cleavage efficiencies more accurately. Following incubation, cleaved and noncleaved products were quantified through PAGE gel analysis. At 10 mM $MgCl_2$, the canonical trans-ribozymes, 554 and 654, cleave ~ 90% of the target (Figure 4.4A). The mRz with no loop structures cleaves ~ 50% of target. At Mg^{2+} concentrations comparable to physiological levels the activity of the mRz is completely abolished, whereas the canonical ribozymes maintain significant activity.
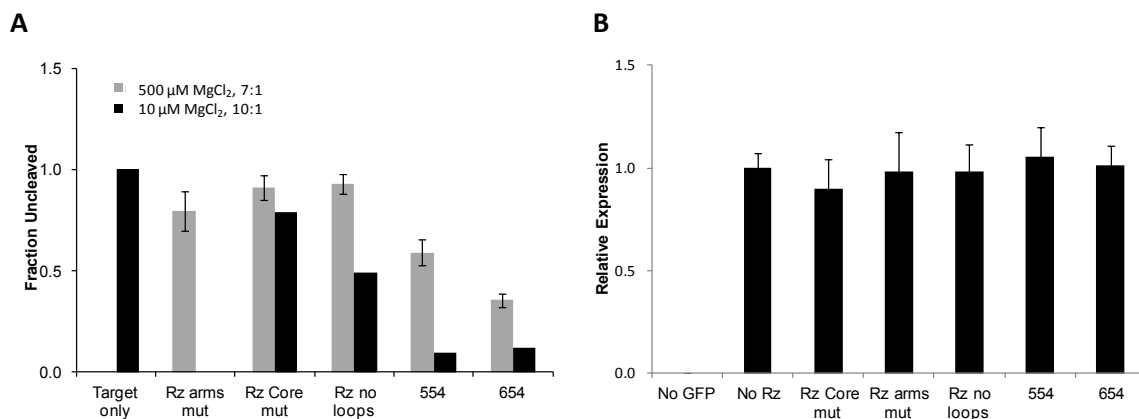
Figure 4.4. Initial ribozyme designs with pCS933. A. *In vitro* cleavage assays after 1 hr at various Mg^{+2} concentrations and ratios of ribozyme to target. **B.** *In vivo* fluorescence levels of yEGFP in various controls and constructs. Relative fluorescence levels were calculated by normalizing mean GFP levels of cells by the mean GFP level of the no ribozyme control. All fluorescence data are reported as the mean ± SD from at least three independent experiments.

We next investigated whether the cleavage activity observed *in vitro* translates to *in vivo* knockdown of target gene expression. In our system, thRzs were expressed from the strong constitutive TEF1 promoter on a high-copy plasmid, pCS933. The yEGFP target sequence fused to a PEST destabilization tag and placed under the control of the TEF1 promoter was integrated into the yeast chromosome. Cellular fluorescence of samples harboring trans-ribozyme expression plasmids and controls was analyzed by flow cytometry and the geometric means of gated cells were calculated (see Methods). Relative expression was calculated by subtracting the mean of the nonfluorescent control and normalizing by the no ribozyme control. The results indicate that despite exhibiting promising *in vitro* activities, these ribozymes did not yield observable knockdown of the target gene when expressed *in vivo* (Figure 4.4B). *In vitro* activity may not translate to *in vivo* knockdown for several reasons. First, our assays capture endpoint cleavage efficiency not kinetic rates of cleavage. Slow cleavage rates may prevent an observable change in gene expression. Alternatively, ribozyme colocalization and hybridization with

the target transcript *in vivo* may be limiting. Given that in the *in vitro* assay we anneal both strands together, the *in vitro* assay may not capture rate limitations with ribozyme-target hybridization and/or nonminimal global free energy states that inhibit the efficiency of hybridization.

Despite the limitations of the assay, the *in vitro* results from the canonical thRzs suggest that cleavage efficiency is limited by the ribozyme-target hybridization. At high Mg^{2+} concentrations the loop interactions should have little effect on the rate of cleavage since sufficient Mg^{2+} is present to stabilize the catalytically active conformation. Thus, observed differences between the mhRz's and the canonical thRzs' cleavage efficiencies at high Mg^{2+} may be a result of differing binding affinities. Increasing the length of the targeting arm is expected to increase the affinity of the ribozyme for its target, facilitating ribozyme-target hybridization. The targeting arms of the mRz are 4 nts and 5 nts shorter than 554 and 654, respectively. At 10 mM, this difference in targeting arm length yields a 40% difference in cleavage efficiency between the mRz and the canonical ribozymes (Figure 4.4A). At 500 μM, the difference in the length of the targeting arms is magnified. Ribozyme 654, which only differs from 554 by a single nucleotide in the targeting arms, is ~ 25% more efficient. These results led us to speculate that increasing the length of the targeting arms may significantly increase the *in vivo* gene-regulatory efficiency of a trans-ribozyme element. In addition to increasing ribozyme affinity for target, increasing the targeting arm length should favor proper ribozyme binding to the target.

Optimization of thRz targeting arms leads to fast, efficient cleavage at physiological MgCl₂ concentrations

To test whether increasing the targeting arms improves ribozyme cleavage efficiency, we constructed three new thRz designs that incorporated longer targeting arms (Figure 4.3B). One design (1154) increased the length of the 5' arm by 5 nts. The second (1154+5) and third (1654) designs built on the first by adding 5 nts to the 3' and 5 nts to the 5' end, respectively (Figure 4.3B). When the resulting ribozyme sequences were folded in RNAstructure 4.3 with the 137 nt target sequence, the proper ribozyme-binding-to-target structure dominated the energy landscape as the minimum free energy (MFE) structure and was the only structure found in the 20 lowest free energy structures (Supplementary Figures 4.1-3). When tested in the *in vitro* ribozyme cleavage end point assays the canonical trans-ribozymes with increased targeting arm length, resulted in greater than 90% cleavage of the target transcript at physiological Mg^{2+} concentrations (Figure 4.5A). Furthermore, the thRzs with increased targeting arm length (1154, 1154+5, 1654) exhibit greater cleavage efficiencies at low Mg^{2+} concentrations than the previous canonical thRz design (554, 654) at higher Mg^{2+} concentrations. These results support that the limiting step in the cleavage reaction is the intramolecular binding event between the thRz and target sequences. Formation of the catalytically active conformation appears to occur readily once the target is found as indicated by the difference between 654 and 1154. However, increased targeting arm lengths may also contribute to increased cleavage efficiency by increasing the stability of the active tertiary conformation as well as the formation of the correct secondary structure. Additionally, the *in vitro* cleavage assays demonstrate that lengthening the targeting arms facilitates

very rapid cleavage of target transcript (Figure 4.5A). Within 10 minutes, all of the

redesigned thRzs reach 97% cleavage efficiency or higher, while even after an hour thRzs

with shorter arms showed 90% or less cleavage efficiency. For *in vivo* application it is

important that the ribozymes act on biologically relevant time scales (~several minutes).

While previous *in vitro* studies have demonstrated fast and efficient thRz cleavage at

higher Mg^{2+} concentrations (1 mM), these results suggest that full-kinetic evaluation will

prove these thRzs to be highly efficient at 500 μM (on the order of minutes).
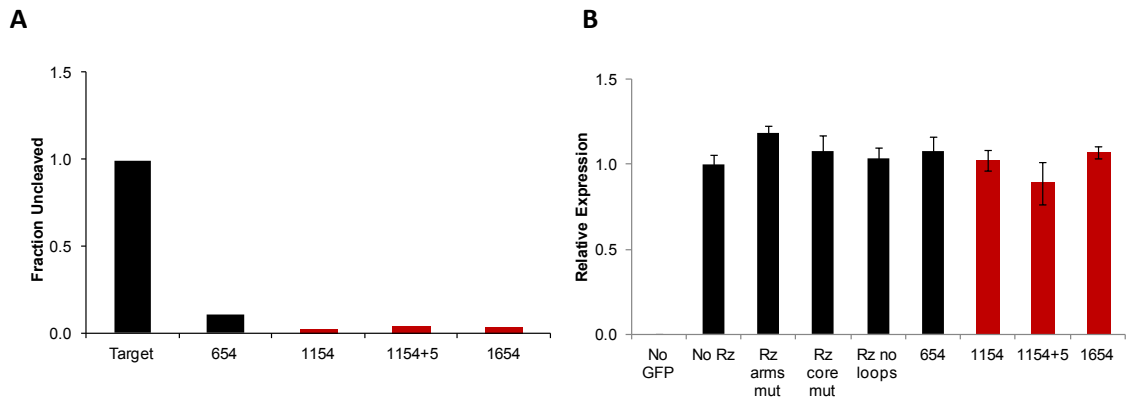
Figure 4.5. Initial ribozyme designs with extended targeting arms show improved *in vitro* efficiency but fail to knockdown expression *in vivo*. A. *In vitro* cleavage assay after 10 minutes at 500 uM Mg^{+2}. **B.** *In vivo* fluorescence levels of yEGFP in various controls and constructs. Relative fluorescence levels were calculated by normalizing mean GFP levels of cells by the mean GFP level of the no ribozyme control. All fluorescence data are reported as the mean ± SD from at least three independent experiments.

The gene-regulatory activities of the thRzs with lengthened targeting arms were

assayed *in vivo* as described previously from the pCS933 expression system. However,

despite very promising *in vitro* results, these optimized trans-ribozymes did not yield

observable knockdown of the target gene when assayed in the *in vivo* expression system

(Figure 4.5B). We suspect that topological constraints on the ribozyme transcript may

hinder ribozyme-target binding, potentially explaining the lack of observable cleavage

activity of these ribozymes *in vivo.* The ribozymes are expressed from a Pol II promoter,

such that during transcription, a modified nucleotide called the 5' cap is added to the 5' end of the ribozyme-encoding mRNAs. As protein factors accumulate on the transcript, the cap binds to the poly-A tail and circularizes the transcript. We postulated that in the ribonucleoprotein particle (RNP) ribozymes may be inhibited from binding to the target transcript by the topological constraints imposed by circularization of the transcript and binding of proteins to the transcript. For example, ribosome loading onto the transcript through the 5' cap structure may occlude the targeting arms from being free to interact with the target transcript.

Implementation of a novel expression system improves the knockdown efficiency of the trans-ribozyme elements

To test whether knockdown could be improved by preventing topological constraints imposed during transcript circularization, we designed and constructed an expression cassette that would allow the thRz to be separated from the RNP. Specifically, two cis-acting hammerhead ribozymes (chRzs) were placed on either side of the thRz element (into pCS933 at AvrII and SacII restriction sites) (Figure 4.5). This new thRz expression cassette contains two chRz, previously shown to be highly efficient at self-cleaving *in vivo* [11, 15], separated by two unique restriction sites, SacI and SphI, for the rapid cloning of the thRz between these two elements (pCS975). The chRzs are expected to excise the thRz from the RNP through self-cleavage, resulting in removal of the transcript tails containing the 5' cap and the poly-A tail. Removal of the 5' cap and poly-A tail will also prevent ribosomes from loading onto the transcript. Additionally, by isolating the liberated transcript from promoter- and terminator-specific transcript tails,

the chRz processing cassette is expected to facilitate thRz portability across a range of expression systems.
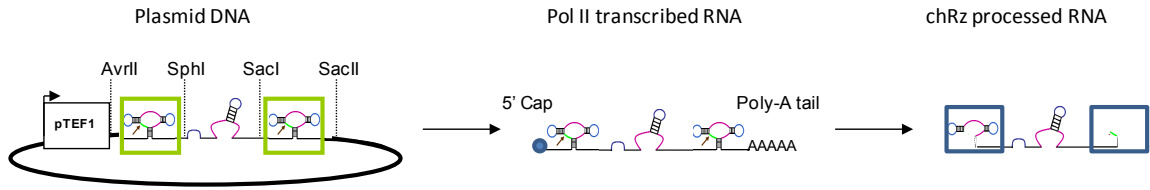
Figure 4.6. Redesigned expression system. The chRz processing cassette was cloned into pCS933 at AvrII and SacII sites to create pCS975. thRz were subsequently cloned between SphI and SacI. pCS975 expresses the trans-ribozyme with flanking cis-hRz (boxes in green) on either side of the thRz transcript designed. Following transcription the chRZs trim the transcript tails, removing the 5' cap and poly-A tail to yield the chRz-processed RNA. Remaining chRz tails shown in blue boxes.

To test *in vitro* activity of the ribozymes in the context of the new expression system, the ribozymes were transcribed from pCS975 containing the chRz cassette along with promoter- and terminator-tails as described previously. *In vitro* cleavage assays confirmed that the chRzs cleave with near-perfect efficiency during transcription as expected given the high Mg^{2+} concentration of the T7 transcription buffer (data not shown). The resulting thRzs with chRz tails were incubated with target at various Mg^{2+} concentrations. At physiological Mg^{2+} concentrations, the thRzs in the context of the chRz-processing cassette show significant sensitivity to targeting arm length. Activity is completely abolished for the thRz with shorter targeting arms (554, 654), but restored for the thRzs with longer targeting arms (Supplementary Figure 4.4A and Figure 4.7A). Overall, the thRzs flanked by the chRzs demonstrated lower cleavage activity compared to the original expression system while maintaining similar trends in cleavage efficiencies. These data suggest that the chRz tails that remain on the trans-ribozyme transcript following cis-cleavage may interfere with thRz activity especially when the targeting arms are shorter. By investigating the predicted structures of ribozymes folded

with target transcripts in RNAstructure 4.3, we determined that the chRzs' tails are predicted to interfere with thRz binding to the target by preferentially promoting formation of Watson-Crick bonds between the target sequence and the catalytic core (Supplementary Figures 4.5–4.7). The resulting competition between the core region and targeting arms for binding to the target sequence may result in the observed decrease in the activity of the trans-ribozyme elements. This effect may be magnified at low Mg^{2+} concentrations, where proper folding of the ribozyme is not aided by increased levels of this ion.
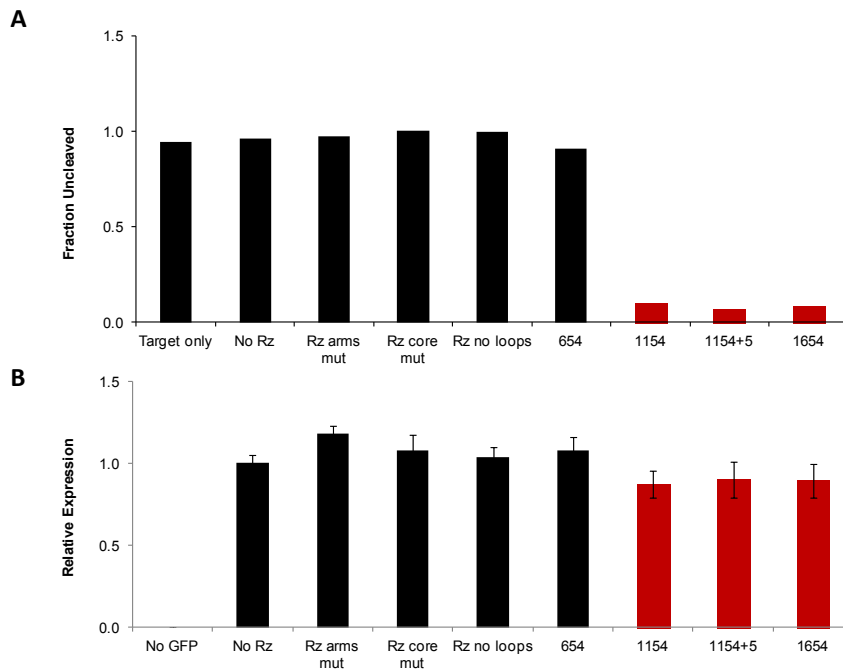
Figure 4.7. Improved ribozymes with chRz-processing expression cassette show only modest *in vivo* knockdown despite significant improvement *in vitro*. A. *In vitro* cleavage assays after 1 hr at 500 uM Mg^{+2}. **B.** *In vivo* fluorescence levels of yEGFP in various controls and constructs. Relative fluorescence levels were calculated by normalizing mean GFP levels of cells by the mean GFP level of the no ribozyme control. All fluorescence data are reported as the mean ± SD from at least three independent experiments.

In vivo assays of ribozyme gene-regulatory activity were performed as described previously to determine if the chRz-processing cassette improved ribozyme-mediated knockdown. *In vivo* expression of the ribozymes from the redesigned plasmid system

demonstrated minimal knockdown of gene expression (~ 10%) (Figure 4.7B). Given that we had established efficient catalytic activity of our designs at low Mg^{2+} concentrations (through the *in vitro* cleavage assays) and modified the design of the expression construct to eliminate potential interference from the RNP and ribosome loading via the chRz processing cassette, we suspected that the *in vivo* gene-regulatory activity of the trans-ribozyme system may be limited by efficient localization and thus hybridization of the trans-ribozyme element to the target transcript in the dense cellular milieu. Additionally, it is possible that by excising the thRzs from the RNP stability of the ribozyme transcript was compromised. Destabilized transcripts would be expected to have short residence times, potentially shorter than the time necessary to locate and hybridize to a target transcript.

Varying target expression levels indicates a biphasic relationship between target concentration and *in vivo* knockdown activity of the trans-ribozyme elements

To determine whether *in vivo* knockdown could be improved by modulating the expression of the target, we modified the *in vivo* assay system such that the level of target transcript could be tuned relative to the level of ribozyme being expressed. It is expected that increasing the level of target transcript will increase the probability of trans-ribozyme binding to the target, thereby potentially increasing ribozyme-mediated knockdown within a particular range of target transcript. Above this range, as ribozymes become saturated by target, knockdown would be expected to taper off and ultimately become unobservable as the rate of binding and cleaving the target transcript is dwarfed by the rate of target expression. Due to these competing effects of target transcript levels, there

may be an optimal level of target expression at which to observe knockdown. Given that

we anticipated that ribozyme saturation could be an issue, the original and improved thRz

expression systems were constructed on a high-copy plasmid with a strong TEF1

promoter to maximize thRz expression. To further increase the ratio of ribozyme to target

we modified the target expression system to allow titration of the target transcript over a

lower range of expression levels. An expression construct encoding the yEGFP gene

regulated from a galactose-inducible promoter, pGAL1, was integrated into the yeast

chromosome to make strain CSY341. Integrating the yEGFP cassette at the GAL2 locus,

converted the all-or-none response of the galactose-inducible promoter to a linear,

homogenous response to galactose as was previously shown [28]. With this modified

expression system the target transcript levels increase as a function of increasing

galactose concentrations. The previous target expression strain CSY132 has yEGFP

integrated with pTEF1 and a PEST destabilization tag. The TEF1 promoter is more than

10 times stronger than the pGAL1 promoter induced with 2% galactose for 6 hours

(Supplementary Figure 4.8).
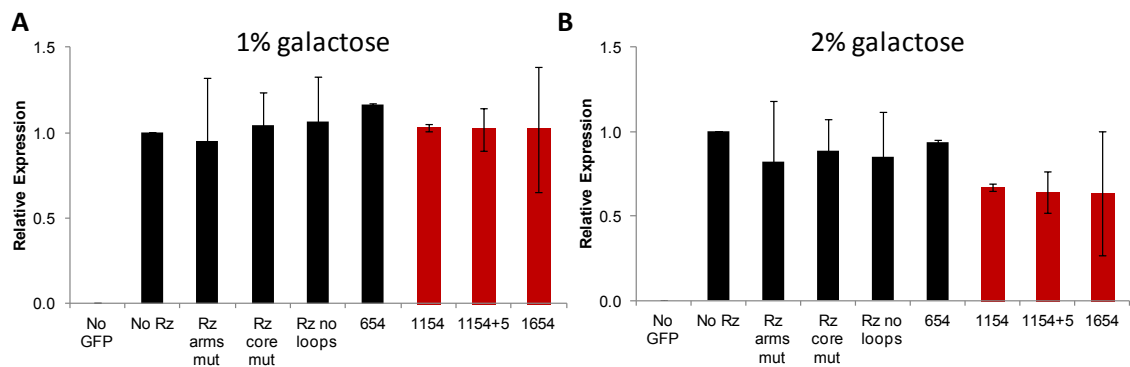
Figure 4.8. Controlling target expression via the galactose-inducible promoter demonstrates that knockdown increases at higher expression levels of target transcript. A. *In vivo* fluorescence levels of yEGFP in various controls and constructs for thRz in chRz-processing expression cassette (pCS975) at 1% galactose and **B**. 2% galactose. Target transcript levels increase with increasing galactose levels. Relative fluorescence levels were calculated by normalizing mean GFP levels of cells by the mean GFP level of the

no ribozyme control. All fluorescence data are reported as the mean ± SD from at least three independent experiments.

We tested the thRz with and without the chRz processing cassette expression system, pCS933 and pCS975, respectively, for *in vivo* knockdown of different levels of target expression. Cells were grown overnight in noninducing, nonrepressing conditions and induced at 1% or 2% galactose for 6 hours before assaying yEGFP via flow cytometry (Materials and Methods). Relative expression was calculated by normalizing to the mean fluorescence of the no ribozyme control at the corresponding galactose concentration. Raw fluorescence means increase on average 3-fold from 1% to 2% galactose. At 1% galactose, ribozyme-mediated knockdown activity is not observed for the thRzs expressed with or without the chRz processing cassette (Figure 4.8A and Supplementary Figure 4.9A, respectively). However, both trans-ribozyme expression systems exhibit improved knockdown ranging from 16%–35% when target gene expression is increased by adding 2% galactose to the cells (Figure 4.8B and Supplementary Figure 4.9B). This data supports the hypothesis that mediating the ribozyme-target binding event is the limiting step *in vivo*.

In evaluating the efficacy of the thRzs across a range of target expression levels, the results indicate that increasing expression levels by ~ 3-fold (from 1% to 2% galactose) increases knockdown from 0% to 35%. However, in the pTEF1-yEGFP-PEST target expression system where expression levels are estimated to be an order of magnitude higher than in the galactose-titratable CYS341 system at 2% galactose, very minimal knockdown is observed (Figure 4.7B). Taken together, these data suggest that ribozyme-mediated knockdown may exhibit a biphasic response to target transcript levels.

Discussion

We have shown that thRzs can be engineered for improved catalytic activity *in vitro* that translates to *in vivo* knockdown dependent on target transcript expression. Through the rational design of the targeting arms aided by computational models of RNA secondary structure, *in vitro* thRz activity at physiologically relevant Mg^{2+} concentrations was significantly increased. Additionally, by modifying our *in vitro* cleavage assay such that the target sequence more accurately reflects the sequence and associated structure targeted *in vivo*, we developed a more instructive *in vitro* cleavage assay for evaluating the potential of thRz designs to efficiently cleave target transcripts at physiologically relevant Mg^{2+} concentrations. Results from the improved *in vitro* assays indicate that increasing targeting arm length improves thRz cleavage efficiency. Further, at these lower Mg^{2+} concentrations, our *in vitro* results support that the designed thRzs efficiently cleave the target on biologically relevant timescales. We observed that implementation of a chRz processing cassette that releases the thRz from the RNP facilitates modest knockdown of the target *in vivo*, an improvement over our initial expression system. Finally, varying target expression levels suggests that ribozyme-mediated knockdown *in vivo* is highly sensitive to target expression levels and responds biphasically to increasing target expression.

To capture binding constraints imposed by the structures formed by the sequences flanking the target sequence on the target transcript, we modified our *in* vitro assay to analyze cleavage of a longer target sequence. Previous *in vitro* analysis of trans-ribozyme efficiency evaluated ribozymes targeting transcripts that were 18 nts in length, such that

the targeting arms hybridized to all but one nt of the sequence [20]. In our modified assay we transcribed 137 nts of the target sequence with 86 and 51 nts on either side of the cleavage site. We anticipated that a target of this length would capture local interactions of the target sequence with the flanking sequence, thus providing us with an assay that captures potential limitations to ribozyme hybridization and cleavage that may exist in the *in vivo* conditions. While previous assays utilizing short target sequences showed that canonical ribozymes with short targeting arms rapidly achieve high cleavage efficiencies (> 90% in 5 minutes) at low Mg^{2+} concentrations [20], our results with the longer target transcript demonstrate that increased targeting arm length was required for similarly efficient cleavage. Further, only thRzs with elongated arms achieved observable knockdown *in vivo*, suggesting that assaying thRz with longer target transcripts improves the translation of cleavage efficiency observed *in vitro* to knockdown observed *in vivo*

Despite improving the ability of the *in vitro* assay to capture the impact of longer target transcripts on cleavage efficiency, the assay could be further improved to mimic the additional constraints imposed by the *in vivo* environment on thRz binding and cleavage. Assays were performed at 50 mM Tris-Cl pH 7.0, 100 mM NaCl at different $MgCl_2$ concentrations as described in previous work [20]. This reaction buffer is unlikely to model the crowded cellular environment. Supplementing the buffer with PEG and/or BSA could potential provide a closer model of the dense cellular milieu in which ribozymes and target transcripts must hybridize. Additionally, since we performed our assays by annealing the ribozyme and target sequences together following purification, the assay could be improved by separately annealing the sequences. *In vivo* ribozymes and target transcripts are transcribed and folded independently, which is likely to result in

important intramolecular structures that can influence ribozyme-target binding. To more accurately represent potential limitations to hybridization of the thRz and target transcript that arise in the intracellular folding environment, individual annealing steps to remove entrapped, nonminimal energy structures induced during the purification step can be performed prior to combining the transcripts or potentially dispensed with all together. While it is desirable to cotranscribe ribozymes with the target, the composition of T7 transcription buffer precludes assessing cleavage efficiency at low Mg^{2+} concentrations, an important requirement for accurately modeling the effect of the intracellular environment on cleavage efficiency.

We demonstrated that the chRz-processing expression system modestly improves knockdown over the original system at high target expression levels. However, no significant difference is observed at low target expression between the two ribozyme expression systems examined in this study. Because the chRz-processing cassette removes the 5' cap and poly-A tail that acts to stabilize transcripts, this expression system may reduce the half-life of expressed thRzs *in vivo*. One explanation for the observed behavior is that at high target expression levels, removing the topological constraints imposed by the RNP may improve ribozyme hybridization rates such that a reduced half-life is less consequential. However, at lower target expression levels, where the average time to bind to a target sequence is expected to increase, thRz half-life may more significantly impact knockdown efficiency and erase efficiencies gained from removing topological constraints associated with the RNP. The expression system might be further improved by the addition of strong hairpin elements at the 5' and 3' ends of the thRz. Such hairpins can increase the residence time of transcripts by protecting against

exonuclease degradation [29, 30]. In addition, spacer regions can be designed to separate the hairpins from the thRz, which may allow for greater insulation of the thRz targeting arms from any bound nucleases or other proteins. Expression systems that can prevent proteins from occluding the thRz targeting arms and increase thRz half-life may result in improved knockdown efficiency.

Varying the levels of the target indicated that ribozyme-mediated knockdown exhibits a biphasic dependence on target expression levels. Specifically, at very low expression levels, no knockdown is observed. Increased expression (3-fold) above this low level results in an increase in the observed knockdown, suggesting that *in vivo* the intramolecular binding event may be limiting knockdown at low target concentrations. However, increasing expression by an order of magnitude reduces observable knockdown potentially due to the target transcript saturating the available ribozyme pool. Probing the range and threshold of target expression for which knockdown is observed could provide a better understanding of the optimal range of target expression levels for thRzs. Delineating this response curve to target expression levels would be useful in identifying potential systems in which trans-acting ribozymes may be effectively applied as regulators of gene expression. The range and threshold of target expression permitting thRz-mediated knockdown are likely to be sequence-specific, thus it would be important to identify a high impact set of targets for ribozyme-mediated knockdown. We did not further probe the threshold and range in our system due to a few system limitations. One drawback of the galactose-titratable system is the inherent noisiness of the galactose promoter. For some samples such as pCS975 1654 (Figure 4.8B), the replicate variability did not allow for significant differentiation from the controls given the error associated

with the assay and system. A more comprehensive and precise study of the relationship between knockdown and target expression levels could be performed by assaying thRz gene-regulatory activities in strains in which the target is expressed from constitutive promoters of varying strength and integrated into the chromosome.

While we have addressed several potential limitations to ribozyme-mediated knockdown, there remain several additional avenues that should be explored to further improve knockdown efficiency. Previous *in vivo* work with thRzs has shown success in targeting the HIV-1 transcript, which is localized to the nucleolus [4]. Researchers used an expression system that localizes thRzs to the nucleolus in order to achieve substantial knockdown of HIV-1 transcripts. Thus, developing a mechanism to localize ribozymes to the target transcript may broadly improve knockdown across a range of target transcript levels. While for many endogenous genetic targets it is not possible to colocalize sequences to cellular substructures, this strategy may be effective for particular systems in which transcripts localize to specific parts of the cell. Additionally, the localization constraints for transcripts may position trans-ribozymes as effective regulators within the context of synthetic gene networks where transcript colocalization can be mediated via expression of the trans-ribozyme and target transcript from the same vector. One final consideration in developing ribozymes as effective regulators of gene expression is the accessibility of the target sequence. Several studies have examined the accessibility of sequences within transcripts for binding to nucleic acids and developed algorithms that predict sequences that exhibit enhanced binding accessibility [31-33]. The utilization of such algorithms may improve the design of trans-acting ribozymes by identifying accessible target sequences.

While the development of a trans-ribozyme platform represents an opportunity to regulate the expression of target transcripts without the need to modify existing, endogenous cellular components, such as binding sites, promoters, repressors, and other cis-acting regulatory elements, or saturating the natural regulatory RNAi pathway, the limited activity observed from these systems *in vivo* constrain the potential applications of this system. Based on these studies, systems with moderately high levels of target transcript that require only modest levels of knockdown are potential candidates for thRz regulation. For example, diseases such as cancer and Alzheimer's are characterized by aberrantly high mRNA levels of particular genes [7, 34, 35]. In Her2 positive cancer cells, overexpression of the Her2 receptor leads to increased cellular growth via upregulation of the signaling pathway [35]. High Her2 expression negatively correlates with survival rates in endometrial cancer [34]. Monoclonal antibodies that target the Her2 receptor reduce tumor proliferation and increase survival rates presumably by binding to Her2 and blocking signaling. Further, siRNA knockdown of Her2 sensitizes cells to monoclonal antibody therapy [34]. However, the systemic administration of these antibodies has resulted in lethal side-effects such as cardiac dysfunction [36]. Broad distribution of these antibodies particularly to cardiac tissue is suspected to reduce signaling critical to preventing cardiac myopathy [35]. To improve therapies for Her2 positive cancers, a thRz targeting the overexpressed Her2 transcripts could provide a therapy targeted to diseased cells. At high Her2 levels, a modest yet potentially significant knockdown of the target transcript could reduce aberrant signaling and additionally sensitize cells to monoclonal therapy. Further, such thRz therapies could

prevent lethal side effects by remaining inert in the case of lower expression levels characteristic of healthy cells.

There remain several challenges in developing such a therapy. First, the expression levels of target transcripts in healthy and diseased cells would need to be determined and evaluated. To reduce expression in diseased cells, expression must be above the requisite threshold for trans-ribozyme-mediated knockdown, but not so high as to saturate the ribozymes present in the cell. Additionally, to optimally differentiate healthy and diseased cells and limit side-effects, expression levels for each cell type should fall below and above the minimum threshold, respectively. Second, utilizing the principles elucidated above, various thRzs would need to be designed to the target transcripts. Utilizing previously mentioned algorithms may aid in the identification of accessible target sites within the transcript. Thirdly, the threshold for knockdown would need to be evaluated to determine if significant knockdown of the targets can be achieved in the diseased cells and if there are any potential effects on healthy cells. It would be useful to determine if the threshold of target transcript knockdown can be tuned via the design of the targeting arm lengths, such that transcripts across a broad range of concentrations can be targeted, increasing the range of potential systems to which these thRzs could be applied. Additionally, differences in metabolism, particularly those affecting transcript degradation and translation rates, may alter the *in vivo* efficiency of thRzs between organisms. This consideration may explain why previous examples of thRzs *in vivo* knockdown have been mostly limited to higher eukaryotes [22, 25]. Finally, ligand-mediated control of ribozyme activity would be a useful tool in directing thRzs as a therapeutic agent. However, the limited efficiency observed in our *in vivo* test

system implies that the current designs would not be amenable to switch construction. While the rules for construction of ligand-responsive switches from chRzs are expected to be readily transferable to thRzs, constructing switches requires appending sequences to the thRz stem II loops. In chRzs, appending sequences to the stem II loops has been shown to reduce cleavage efficiency compared to the nonswitch control [26]. For the successful construction of ligand-responsive thRz switches, ribozymes are anticipated to require higher *in vivo* activity than those developed in this study to target yEGFP.

While significant progress has been made in understanding the catalytic behavior of trans-acting ribozymes *in vitro* in this work and others [17, 18, 20], this progress has not yet been translated beyond modest *in vivo* gene regulation. Given the success of cis-acting ribozymes *in vivo,* the key limitation to efficacy of trans-acting ribozymes appears to be facilitating the intermolecular hybridization interaction between the trans-ribozyme and target mRNA sequences. While this limits the potential application space of trans-acting ribozymes, it may position these devices as uniquely targeted regulators of gene expression for systems requiring modest knockdown of targets that are overexpressed and near quiescence at normal low levels. Additionally, trans-ribozymes may be useful control tools within synthetic circuits where there exists greater design flexibility for mediating transcript colocalization. Future work on these devices should focus on identifying potential systems for application and designing thRz to function in these systems as biochemical controllers of gene expression.

Materials and methods

Plasmid and ribozyme construction

Standard molecular biology cloning techniques were used to construct all plasmids [37]. DNA synthesis was performed by Integrated DNA Technologies (Coralville, IA). All enzymes, including restriction enzymes and ligases, were obtained through New England Biolabs (Ipswich, MA). Ligation products were electroporated with a GenePulser XCell (Bio-Rad, Hercules, CA) into an *E. coli* DH10B strain (Invitrogen, Carlsbad, CA), where cells harboring cloned plasmids were maintained in Luria-Bertani media containing 50 mg/ml ampicillin (EMD Chemicals). All cloned constructs were sequence verified by Laragen Inc (Santa Monica, CA).

The thRz expression constructs, pCS933 and pCS975, were constructed from pCS346 (Supplementary Figure 4.10). pCS346 bears two sets of TEF1 promoters and CYC1 terminators with intervening unique restriction sites. Briefly, pCS933 was constructed by cloning a version of RFP (tdimer2), which served as a transformation control signal, into the SalI and NotI restriction sites downstream of the second TEF1 promoter in pCS346. Site-directed PCR mutagenesis was performed to remove the two SacII sites from tdimer2, preserving SacII as a unique restriction site using the QuikChange II Site-directed mutagenesis kit (Agilent, Santa Clara, CA) according to manufacturer instructions. The pCS933 engineered ribozyme constructs were generated by cloning the appropriate thRz constructs into the unique restriction sites, AvrII and SacII, downstream of the first TEF1 promoter (see Supplementary Table 4.1 and Supplementary Table 4.2). The thRz with flanking chRzs plasmid, pCS975, was constructed by cloning a cassette containing two chRz with two intervening unique

restriction sites, SphI and SacI, into AvrII and SacII using the primers Cis-Cis.sTRSV.FWD and Cis-Cis.sTRSV.REV. The pCS975 engineered ribozyme constructs were generated by cloning the appropriate thRz constructs into the SphI and SacI sites. All oligonucleotides were synthesized by Integrated DNA Technologies (Coralville, IA). Cloned plasmids were transformed via electroporation into an electrocompetent *Escherichia coli* strain, DH10B (Invitrogen, Carlsbad, CA), and all cloned ribozyme constructs were confirmed by sequencing (Laragen, Los Angeles, CA).

Confirmed plasmid constructs were transformed into CSY132, a *S. cerevisiae* W303 strain harboring a chromosomally integrated pTEF1-yEGFP-PEST target construct (*MATα his3-11,15 trp1-1 leu2-3 ura3-1 ade2-1, pTEF1-yEGFP-PEST*) or CSY341, a *S. cerevisiae* W303 strain harboring a chromosomally integrated pGAL1-yEGFP target construct (*MATα his3-11,15 trp1-1 leu2-3 ura3-1 ade2-1, Δgal2, pGAL1-yEGFP*) using a standard lithium acetate procedure (Supplementary Table 4.3) [38]. To construct CSY341, the pGAL1-yEGFP cassette was PCR amplified from pCS1340 (Supplementary Figure 4.11) using primers GAL2ko.fwd and GAL2ko.rev to integrate the cassette at the GAL2 locus (Supplementary Table 4.4). Yeast strain CSY3 was transformed as described previously with 12 μg of gel purified PCR product and plated on G418 plates to build yeast strain CSY341.

***In vitro* endpoint cleavage assays**

All ribozymes were PCR amplified from their plasmids beginning at 23 nts upstream from the TEF1 promoter using primers T7Rbz 5'-23.FWD and T7Rbz 3'.REV (Supplementary Table 4.5). A 137 nt region of the target yEGFP sequence was amplified

by PCR using Target.yEGFP.FWD and Target.yEGFP.REV, where the forward primer in each of these amplification reactions harbors the T7 polymerase sequence at its 5' end. PCR products were transcribed using an Ampliscribe T7 kit (Epicentre Technologies, Madison, WI) according to manufacturer's instructions. Transcription reactions were DNaseI treated for 15 min. at 37°C and purified into reaction buffer (50 mM Tris-Cl pH 7.0, 100 mM NaCl, and the specified MgCl$_2$ concentration) through a NucAway column (Ambion, Foster City, CA) following the manufacturer's instructions. The target transcript was radiolabeled by modifying the reaction solution to include 2 µl of [α-32P]-GTP and 1 µl GTP. Cleavage reactions were performed in a 20 µl total volume at 50 mM Tris-Cl pH 7.0, 100 mM NaCl, and the specified MgCl$_2$ concentration. The ratio of ribozyme to target was 10:1 and 7:1 was specified by varying the volume of purified ribozyme and target RNA added to reactions. The ribozyme and target sequence were annealed in reaction buffer by incubating at 95°C for 5 min and cooling at room temperature for 15 minutes. Reactions were run at 37°C for either 10 or 60 minutes and quenched with the addition of RNA loading buffer II (Ambion). Prior to loading on the gel, reaction products were heated at 65°C for 5 minutes and chilled at 4°C for 5 minutes. The reaction products were separated on a 6% denaturing PAGE gel, dried, and visualized on a FX phosphorimager (Bio-Rad, Hercules, CA). The RNA decade ladder (Ambion Foster City, CA) was used as a size marker. The background-subtracted intensity of full-length target (137 nt) and cleaved products (~50 and 85 nts) were quantified for each sample using the Quantity One software package (Bio-Rad). The fraction of RNA uncleaved was determined by dividing the intensity of full-length target by total intensity.

In vivo ribozyme characterization assays

  S. cerevisiae cells (W303) harboring the appropriate plasmids were grown in synthetic complete medium supplemented with an appropriate dropout solution and sugar [2% (wt/vol) dextrose] overnight at 30°C. For galactose titration, 2% raffinose and 1% sucrose were substituted for dextrose. Overnight cultures were back-diluted into fresh medium to an optical density at 600 nm (OD_{600}) of ~ 0.1 and grown at 30°C. For galactose titration experiments, cells were back-diluted into fresh medium containing the specified galactose concentration. Cells were grown for 6 hours (~ OD_{600} of 0.8–1.0) before measuring GFP levels on a Cell Lab Quanta SC flow cytometer (Beckman Coulter, Fullerton, CA).

Fluorescence quantification

  Population averaged fluorescence values were measured on a Quanta flow cytometer with the following settings: 488 nm laser line, 525 nm bandpass filter, and photomultiplier tube setting of 7.53 on FL1 (GFP) and 6.53 on FL3 (RFP). Fluorescence data were collected under low flow rates for ~ 20,000 viable cells. Cells bearing plasmids not expressing RFP were used to set a "RFP negative" gate. Viable cells bearing the plasmid were selected by gating for cells with fluorescence values on FL3 greater than the RFP negative gate. GFP fluorescence levels were determined from 10,000 counts in this selected population. Since the pTEF1-yEGFP cassette is integrated into the chromosome, the mean FL1 values from the entire population of viable, RFP positive cells was determined as the sample's GFP expression level. Relative fluorescence levels

were calculated by normalizing mean GFP levels by the mean GFP level of the no ribozyme control. All fluorescence data are reported as the mean ± SD from at least three independent experiments.

Acknowledgements

References

1.   Isaacs FJ, Dwyer DJ, Collins JJ: **RNA synthetic biology.** *Nat Biotechnol* 2006, **24:**545 – 554.

2.   Kobayashi H, Kaern M, Araki M, Chung K, Gardner TS, Cantor CR, Collins JJ: **Programmable cells: interfacing natural and engineered gene networks.** *Proc Natl Acad Sci U S A* 2004, **101:**8414 – 8419.

3.   Fire A, Xu S, Montgomery MK, Kostas SA, Driver SE, Mello CC: **Potent and specific genetic interference by double-stranded RNA in Caenorhabditis elegans.** *Nature* 1998, **391:**806 – 811.

4.   Li MJ, Kim J, Li S, Zaia J, Yee JK, Anderson J, Akkina R, Rossi JJ: **Long-term inhibition of HIV-1 infection in primary hematopoietic cells by lentiviral vector delivery of a triple combination of anti-HIV shRNA, anti-CCR5 ribozyme, and a nucleolar-localizing TAR decoy.** *Mol Ther* 2005, **12:**900 – 909.

5.   Aagaard L, Rossi JJ: **RNAi therapeutics: principles, prospects and challenges.** *Adv Drug Deliv Rev* 2007, **59:**75 – 86.

6.   Grimm D, Streetz KL, Jopling CL, Storm TA, Pandey K, Davis CR, Marion P, Salazar F, Kay MA: **Fatality in mice due to oversaturation of cellular microRNA/short hairpin RNA pathways.** *Nature* 2006, **441:**537 – 541.

7.   Hanahan D, Weinberg RA: **The hallmarks of cancer.** *Cell* 2000, **100:**57 – 70.

8.   Qi M, Elion EA: **MAP kinase pathways.** *J Cell Sci* 2005, **118:**3569 – 3572.

9. McCormick F: **Signalling networks that cause cancer.** *Trends Cell Biol* 1999, **9:**M53 – 56.

10. Long DM, Uhlenbeck OC: **Self-cleaving catalytic RNA.** *Faseb J* 1993, **7:**25 – 30.

11. Khvorova A, Lescoute A, Westhof E, Jayasena SD: **Sequence elements outside the hammerhead ribozyme catalytic core enable intracellular activity.** *Nat Struct Biol* 2003, **10:**708 – 712.

12. Blount KF, Uhlenbeck OC: **The structure-function dilemma of the hammerhead ribozyme.** *Annu Rev Biophys Biomol Struct* 2005, **34:**415 – 440.

13. Salehi-Ashtiani K, Szostak JW: **In vitro evolution suggests multiple origins for the hammerhead ribozyme.** *Nature* 2001, **414:**82 – 84.

14. Hammann C, Norman DG, Lilley DM: **Dissection of the ion-induced folding of the hammerhead ribozyme using 19F NMR.** *Proc Natl Acad Sci U S A* 2001, **98:**5503 – 5508.

15. De la Pena M, Gago S, Flores R: **Peripheral regions of natural hammerhead ribozymes greatly increase their self-cleavage activity.** *Embo J* 2003, **22:**5561 – 5570.

16. Pley HW, Flaherty KM, McKay DB: **Three-dimensional structure of a hammerhead ribozyme.** *Nature* 1994, **372:**68 – 74.

17. Canny MD, Jucker FM, Kellogg E, Khvorova A, Jayasena SD, Pardi A: **Fast cleavage kinetics of a natural hammerhead ribozyme.** *J Am Chem Soc* 2004, **126:**10848-10849.

18. Penedo JC, Wilson TJ, Jayasena SD, Khvorova A, Lilley DM: **Folding of the natural hammerhead ribozyme is enhanced by interaction of auxiliary elements.** *Rna* 2004, **10:**880 – 888.

19. Saksmerprome V, Roychowdhury-Saha M, Jayasena S, Khvorova A, Burke DH: **Artificial tertiary motifs stabilize trans-cleaving hammerhead ribozymes under conditions of submillimolar divalent ions and high temperatures.** *Rna* 2004, **10:**1916 – 1924.

20. Weinberg MS, Rossi JJ: **Comparative single-turnover kinetic analyses of trans-cleaving hammerhead ribozymes with naturally derived non-conserved sequence motifs.** *FEBS Lett* 2005, **579:**1619 – 1624.

21. Weinberg M, Passman M, Kew M, Arbuthnot P: **Hammerhead ribozyme-mediated inhibition of hepatitis B virus X gene expression in cultured cells.** *J Hepatol* 2000, **33:**142 – 151.

22. Weinberg MS, Ely A, Passman M, Mufamadi SM, Arbuthnot P: **Effective anti-hepatitis B virus hammerhead ribozymes derived from multimeric precursors.** *Oligonucleotides* 2007, **17:**104 – 112.

23. Grassi G, Forlino A, Marini JC: **Cleavage of collagen RNA transcripts by hammerhead ribozymes in vitro is mutation-specific and shows competitive binding effects.** *Nucleic Acids Res* 1997, **25:**3451 – 3458.

24. Scherr M, Grez M, Ganser A, Engels JW: **Specific hammerhead ribozyme-mediated cleavage of mutant N-ras mRNA in vitro and ex vivo. Oligoribonucleotides as therapeutic agents.** *J Biol Chem* 1997, **272:**14304 – 14313.

25. Pan WH, Xin P, Morrey JD, Clawson GA: **A self-processing ribozyme cassette: utility against human papillomavirus 11 E6/E7 mRNA and hepatitis B virus.** *Mol Ther* 2004, **9:**596 – 606.

26. Win MN, Smolke CD: **A modular and extensible RNA-based gene-regulatory platform for engineering cellular function.** *Proc Natl Acad Sci U S A* 2007.

27. Michienzi A, Rossi JJ: **Intracellular applications of ribozymes.** *Methods Enzymol* 2001, **341:**581 – 596.

28. Hawkins KM, Smolke CD: **The regulatory roles of the galactose permease and kinase in the induction response of the GAL network in Saccharomyces cerevisiae.** *J Biol Chem* 2006, **281:**13485 – 13492.

29. Alifano P, Bruni CB, Carlomagno MS: **Control of mRNA processing and decay in prokaryotes.** *Genetica* 1994, **94:**157 – 172.

30. Smolke CD, Carrier TA, Keasling JD: **Coordinated, differential expression of two genes through directed mRNA cleavage and stabilization by secondary structures.** *Appl Environ Microbiol* 2000, **66:**5399 – 5405.

31. Reynolds A, Leake D, Boese Q, Scaringe S, Marshall WS, Khvorova A: **Rational siRNA design for RNA interference.** *Nat Biotechnol* 2004, **22:**326 – 330.

32. Heale BS, Soifer HS, Bowers C, Rossi JJ: **siRNA target site secondary structure predictions using local stable substructures.** *Nucleic Acids Res* 2005, **33:**e30.

33. Scherr M, Rossi JJ: **Rapid determination and quantitation of the accessibility to native RNAs by antisense oligodeoxynucleotides in murine cell extracts.** *Nucleic Acids Res* 1998, **26:**5079 – 5085.

34. Mori N, Kyo S, Nakamura M, Hashimoto M, Maida Y, Mizumoto Y, Takakura M, Ohno S, Kiyono T, Inoue M: **Expression of HER-2 affects patient survival and paclitaxel sensitivity in endometrial cancer.** *Br J Cancer* 2010, **103:**889 – 898.

35. Negro A, Brar BK, Lee KF: **Essential roles of Her2/erbB2 in cardiac development and function.** *Recent Prog Horm Res* 2004, **59:**1 – 12.

36. Levine MN: **Trastuzumab cardiac side effects: only time will tell.** *J Clin Oncol* 2005, **23:**7775 – 7776.

37. Sambrook J RD: *Molecular Cloning: A Laboratory Manual, 3rd edn.* Cold Spring Harbor, NY: Cold Spring Harbor Lab Press; 2001.

38. Guthrie C, Fink G: *Guide to Yeast Genetics and Molecular and Cell Biology.* London: Elsevier, Inc.; 2004.
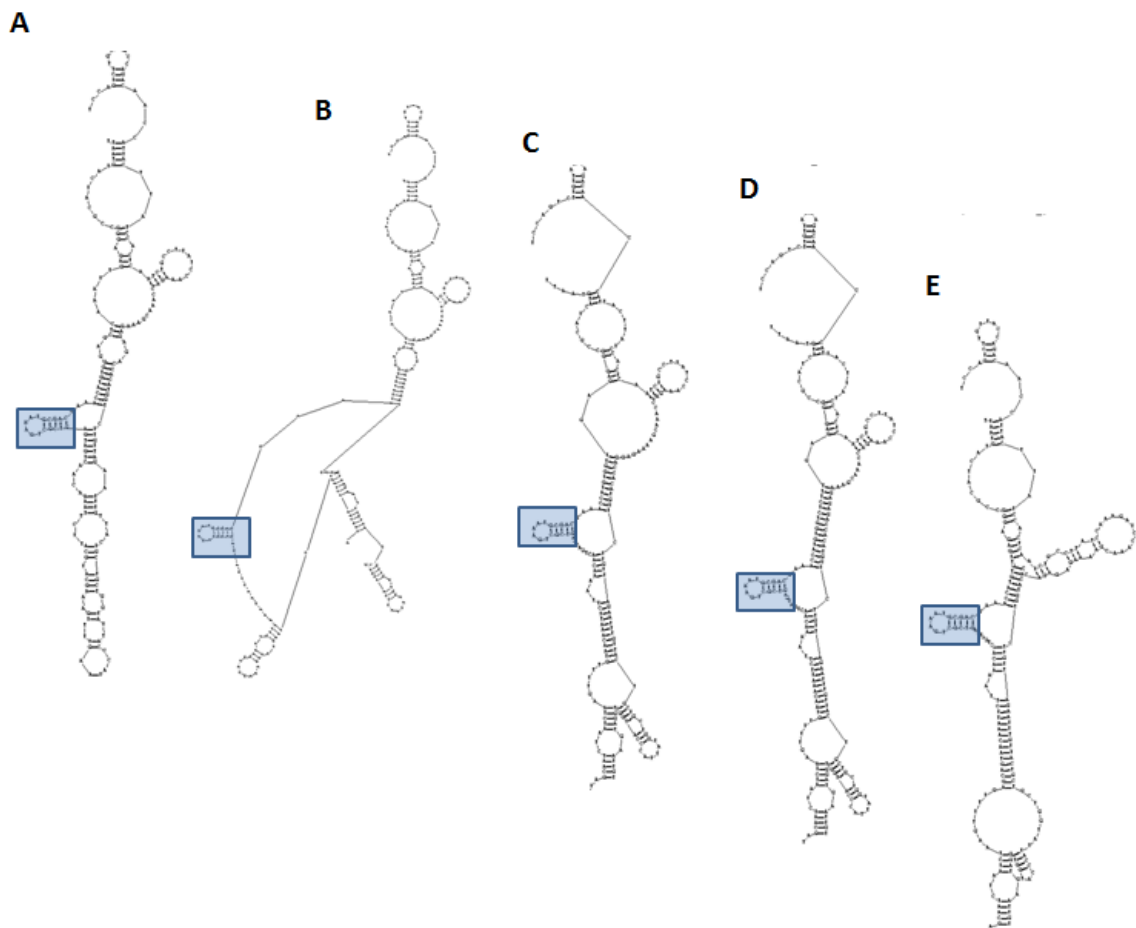
Supplementary figures
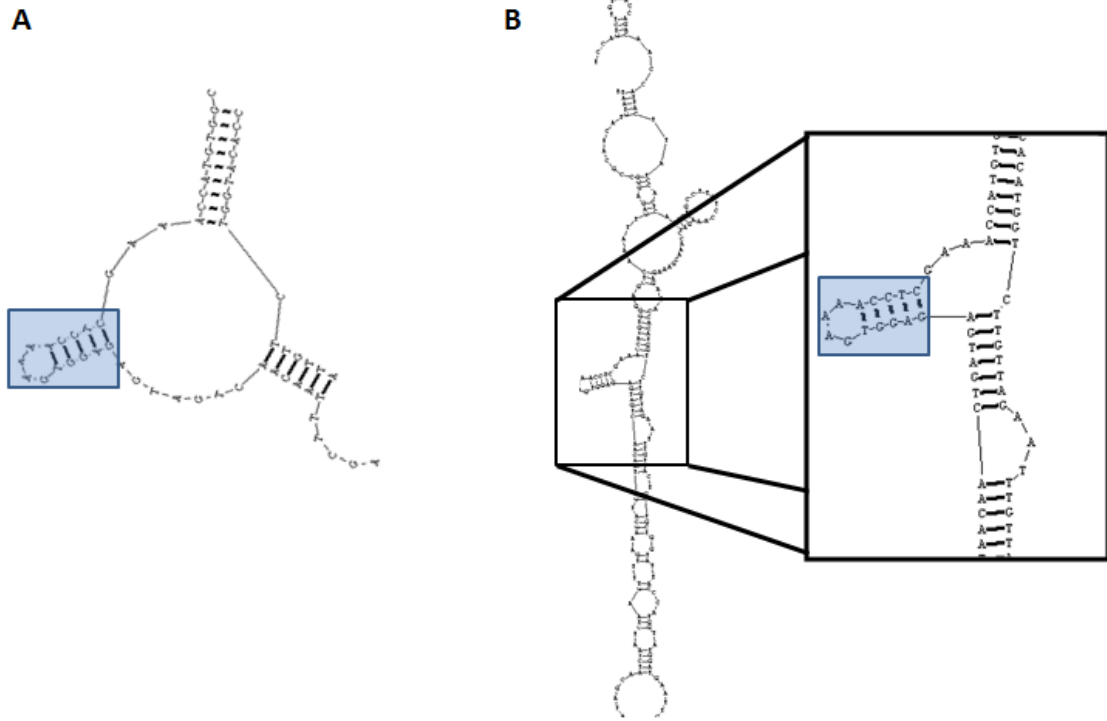
Supplementary Figure 4.1. Comparison of minimal ribozyme folded with truncated and extended target sequence in RNAstructure. A. The minimal ribozyme, SS1, folded without promoter and terminator transcript tails to truncated target sequence shows proper ribozyme-target binding and formation of the catalytic core. **B.** The minimal ribozyme, SS1, folded with promoter and terminator transcript tails from pCS933 to the extended 137 nucleotide (nt) yEGFP sequence shows nucleotides in the catalytic core preferentially binding to target sequence, preventing core formation. Stem II boxed in blue to provide orientation and comparison between figures.
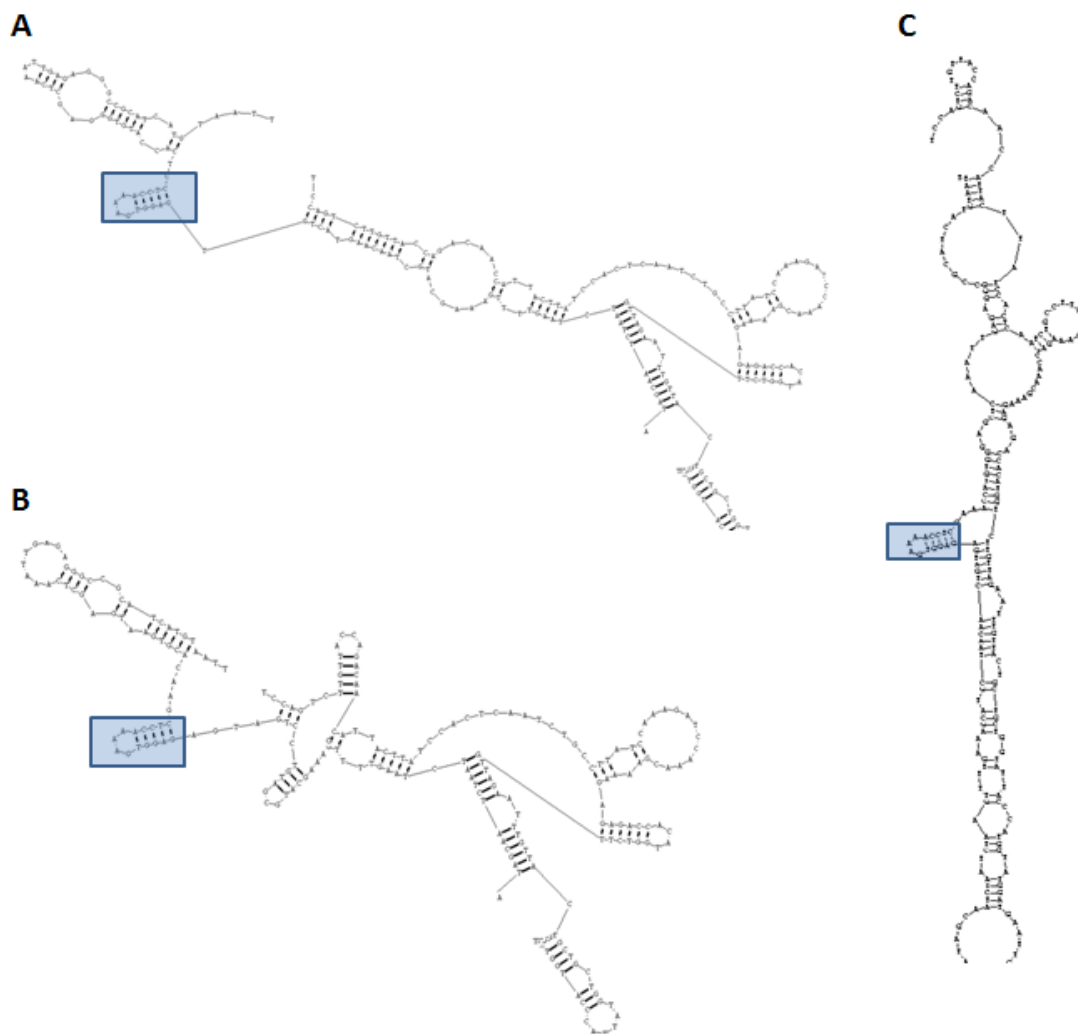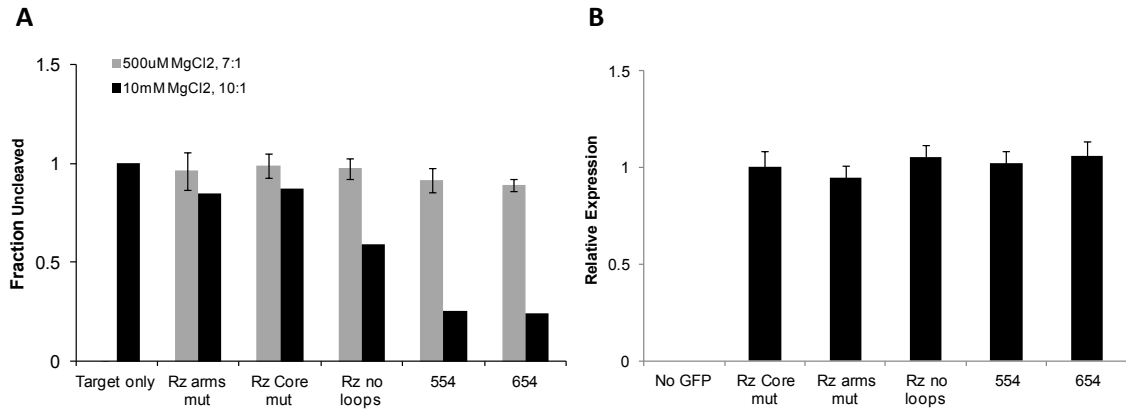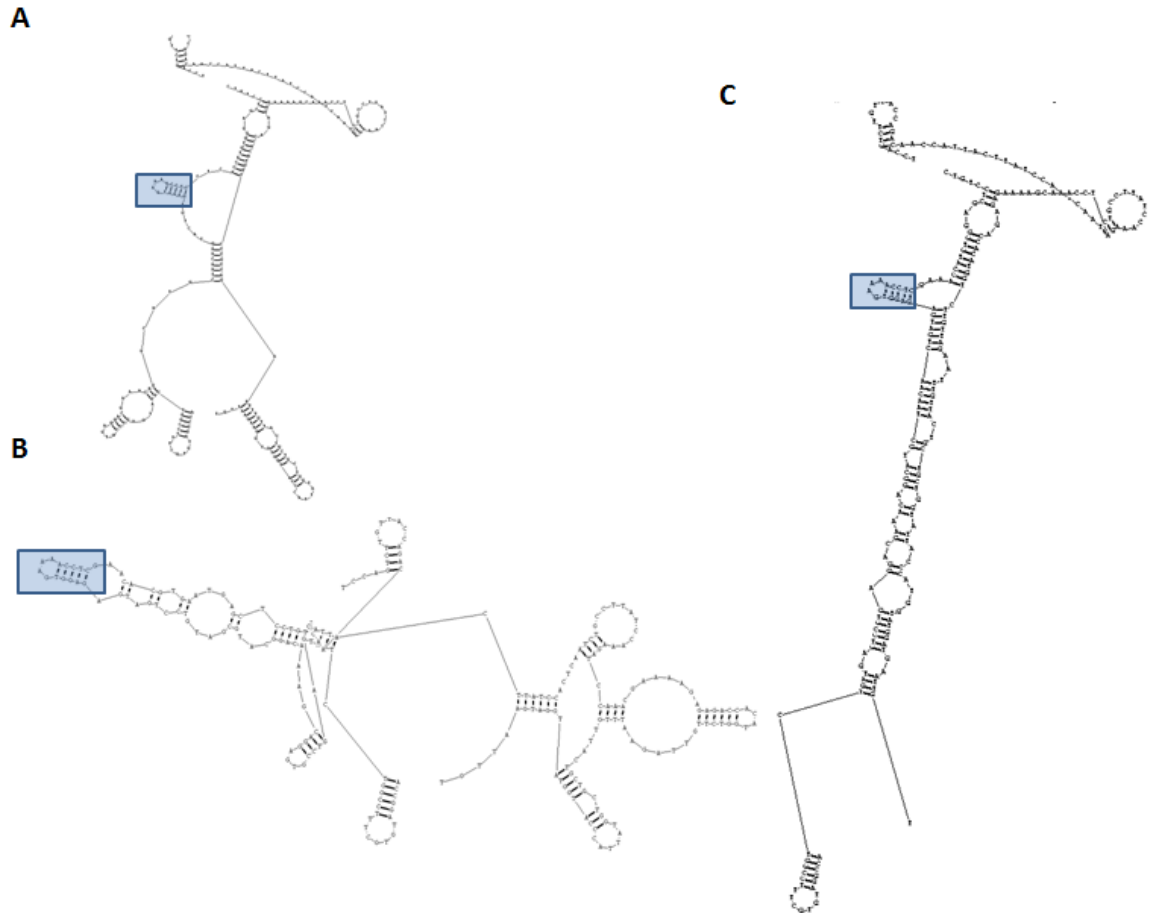
Supplementary Figure 4.2. Control ribozyme sequences from pCS933 folded with extended 137 nucleotide yEGFP target sequence. A. SSCR1, a ribozyme with scrambled core sequence folded with target shows mutated core binding to target sequence. **B.** SSACR, a ribozyme with scrambled targeting arms shows that targeting arms do not properly fold with target. **C.** SS1, a minimal ribozyme without canonical loops, shows nucleotides in the catalytic core binding to target sequence. Stem II boxed in blue to provide orientation and comparison between figures.
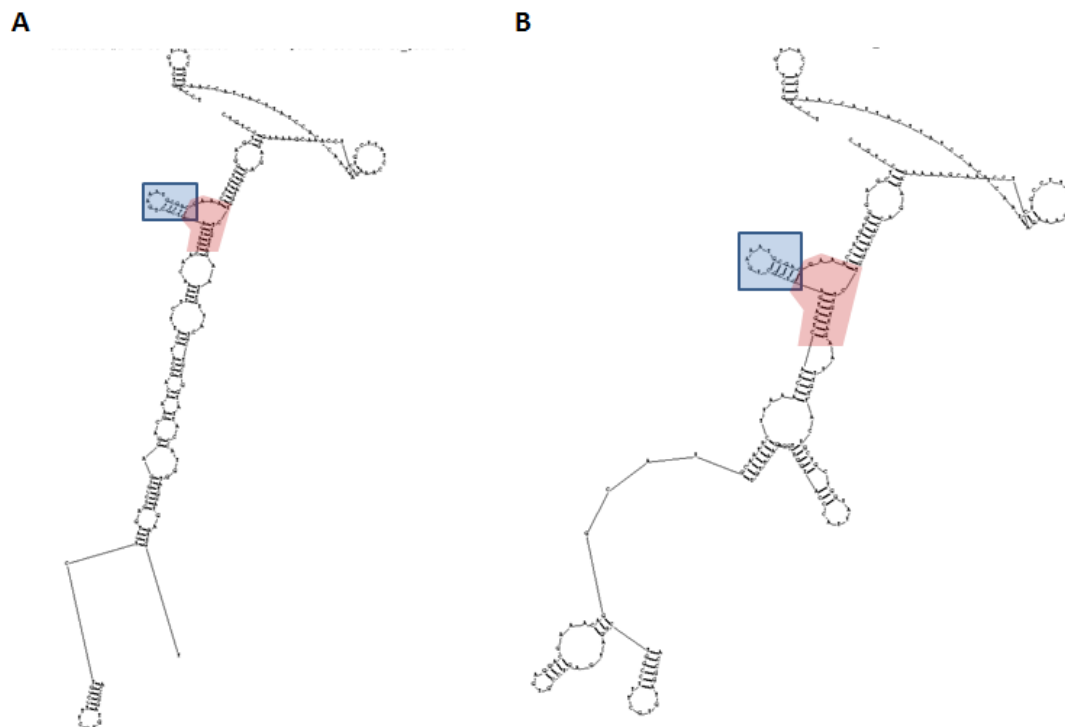
Supplementary Figure 4.3. Canonical ribozyme sequences from pCS933 folded with extended 137 nucleotide yEGFP target sequence. A. 554, a ribozyme with canonical PLMVd stem loops folded with target shows core binding to target sequence. **B.** 654, a ribozyme with canonical PLMVd stem loops folded with target shows 5' targeting arm preferentially binding as a hairpin instead of to target sequence. **C-E.** 1154, 1154+5, and 1654 folded with target show ribozyme binding to target sequence and proper catalytic core formation. Stem II boxed in blue to provide orientation and comparison between figures.

A

B

Supplementary Figure 4.4. Initial ribozyme designs with chRZ processing expression cassette (pCS975). A. *In vitro* cleavage assays after 1 hr at various Mg^{+2} concentrations demonstrate the chRz-processing cassette thRzs are highly sensitive to Mg^{+2} concentrations. **B.** *In vivo* fluorescence levels of yEGFP in various controls and constructs. The initial ribozyme designs are insufficient to knockdown expression *in vivo* as expected from the *in vitro* data. Relative fluorescence levels were calculated by normalizing mean GFP levels of cells by the mean GFP level of the no ribozyme control. All fluorescence data are reported as the mean ± SD from at least three independent experiments.

Supplementary Figure 4.5. Control ribozyme sequences from pCS975 folded with extended 137 nucleotide yEGFP target sequence. A. SSCR1, a ribozyme with scrambled core sequence folded with target shows arms correctly binding target sequence. Mutated core also binds "X" in NUX triplet of target sequence. **B.** SSACR, a ribozyme with scrambled targeting arms shows that targeting arms do not properly fold with target. **C.** SS1, a minimal ribozyme without canonical loops, shows nucleotides in the catalytic core binding to target sequence. Stem II boxed in blue to provide orientation and comparison between figures.

Supplementary Figure 4.6. Canonical ribozyme sequences from pCS975 folded with extended 137 nucleotide yEGFP target sequence. A. 554, a ribozyme with canonical PLMVd stem loops folded with target shows core highlighted in red binding to target sequence. **B.** 654, a ribozyme with canonical PLMVd stem loops folded with target shows core highlighted in red binding to target sequence. Stem II boxed in blue to provide orientation and comparison between figures**.**
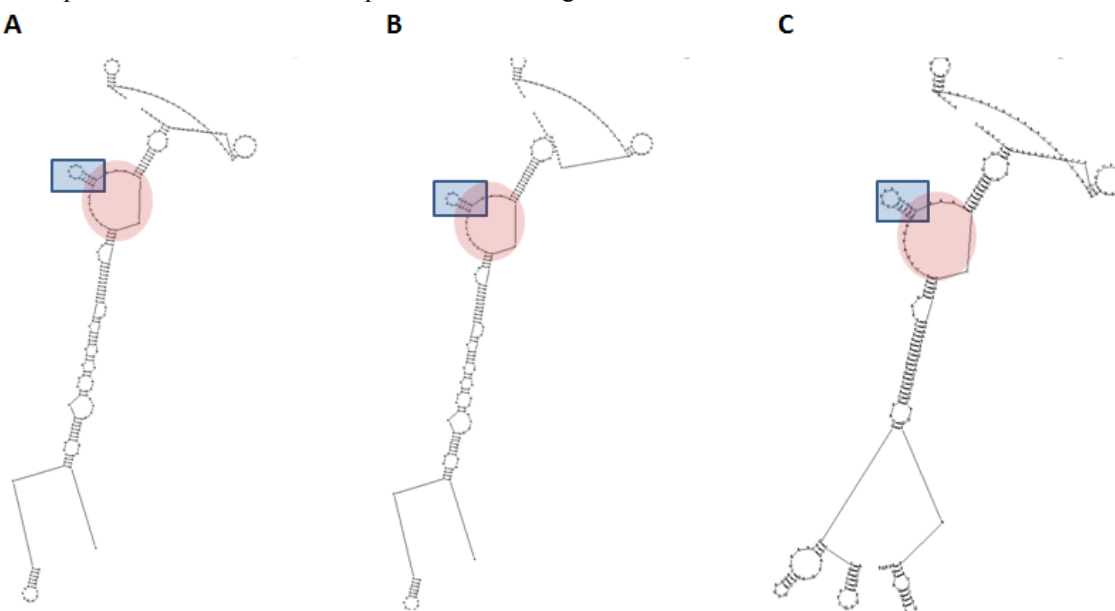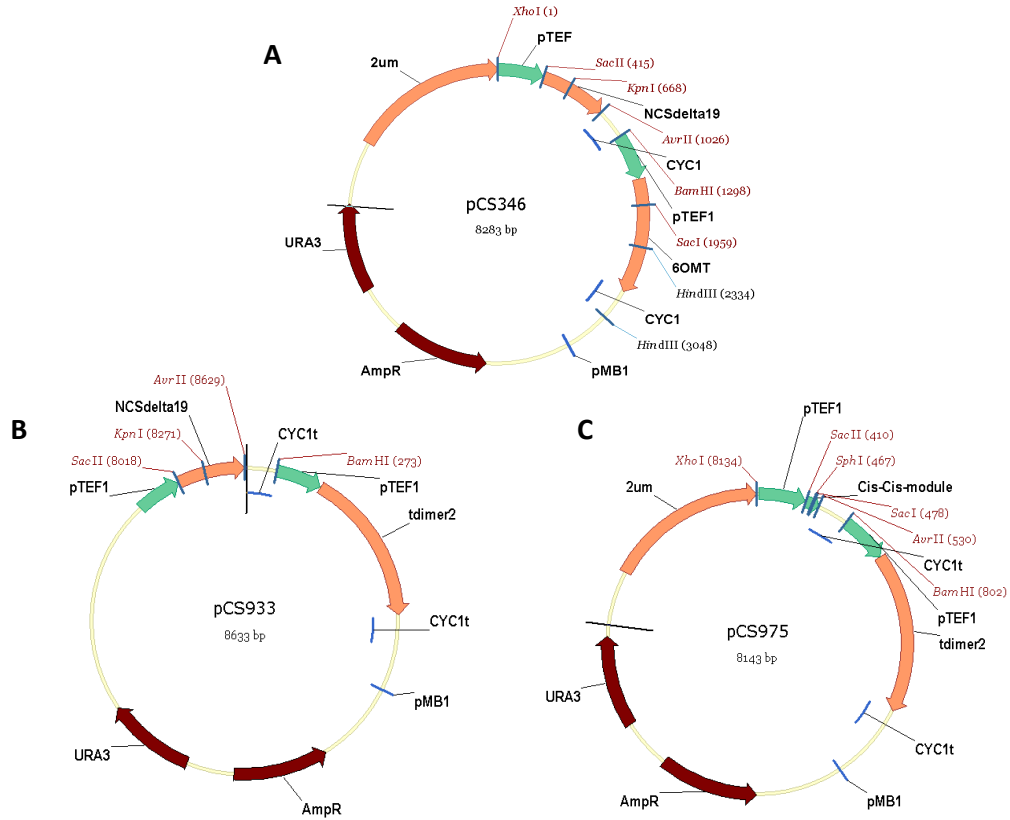

Supplementary Figure 4.7. Canonical ribozyme sequences from pCS975 folded with extended 137 nucleotide yEGFP target sequence. A-C. 1154, 1154+5, and 1654, respectively folded with target show ribozyme binding to target sequence and proper catalytic core formation highlighted in red. Stem II boxed in blue to provide orientation and comparison between figures.
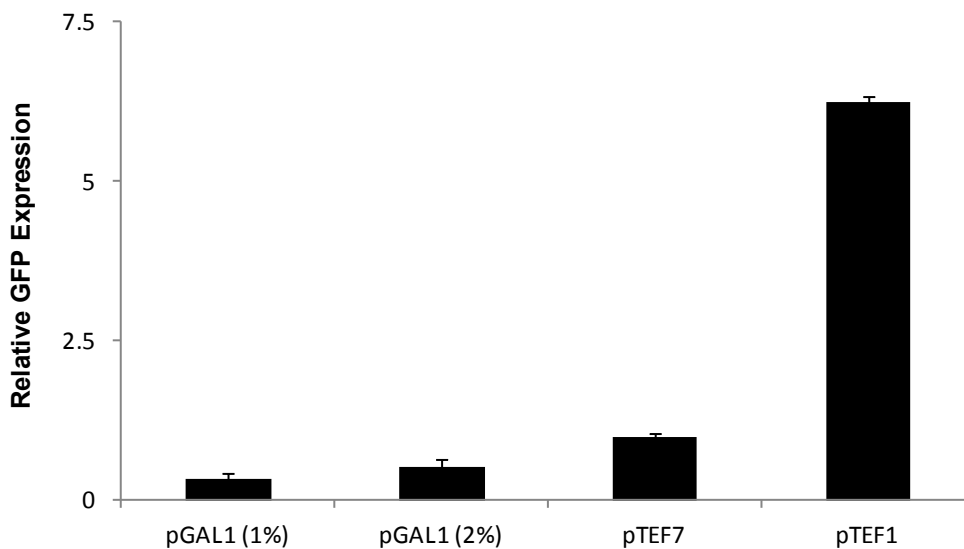
Supplementary Figure 4.8. Promoter characterization. pGAL1 induced at shown percentage of galactose for 6 hours. GFP expression is calculated from the fluorescent geometric mean of viable cells gated above the nonfluorescent control. Expression is shown relative to pTEF7. pTEF1 data from reference for TEF1 library showing pTEF7 is 16% of pTEF1 strength.
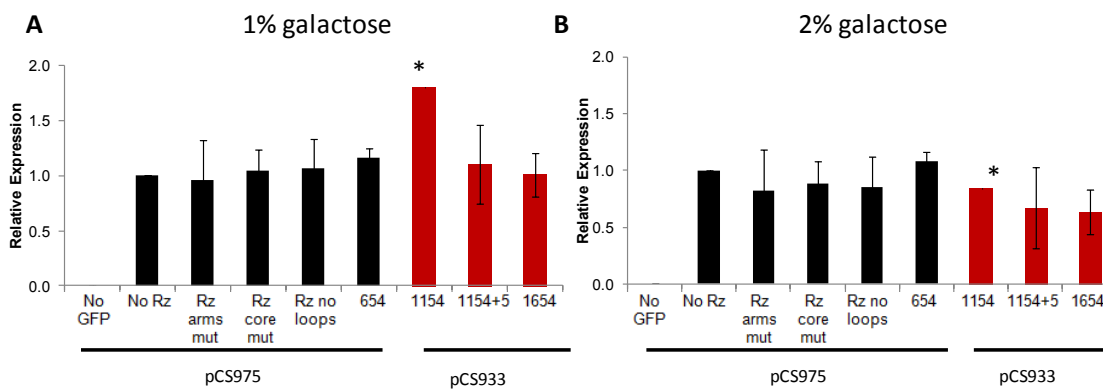
Supplementary Figure 4.9. Ribozyme designs with extended arms in pCS933. A. *In vitro* cleavage assays after 1 hr at various Mg^{+2} concentrations. **B.** *In vivo* fluorescence levels of yEGFP in various controls and constructs. Relative fluorescence levels were calculated by normalizing mean GFP levels of cells by the mean GFP level of the no ribozyme control. All fluorescence data are reported as the mean ± SD from at least three independent experiments, except where a single sample is indicated by * and no error bars.

Supplementary Figure 4.10. Plasmid maps for ribozyme expression vectors. A. pCS346 was previously constructed by K. Hawkins with two expression cassettes with promoter (pTEF1) and terminator (CYC1t) controlling two enzymes NCSdelta19 and 6OMT. **B.** pCS933 was constructed from by cloning a version of RFP, tdimer2, into the SalI and NotI restriction sites downstream of the second TEF1 promoter in pCS346 and served as a transformation control signal. **C.** pCS975 was constructed from pCS933 by cloning a cassette containing two chRz with two intervening unique restriction sites, SphI and SacI, into AvrII and SacII using the primers Cis-Cis.sTRSV.FWD and Cis-Cis.sTRSV.REV to create the cis-processing cassette shown as Cis-Cis module.
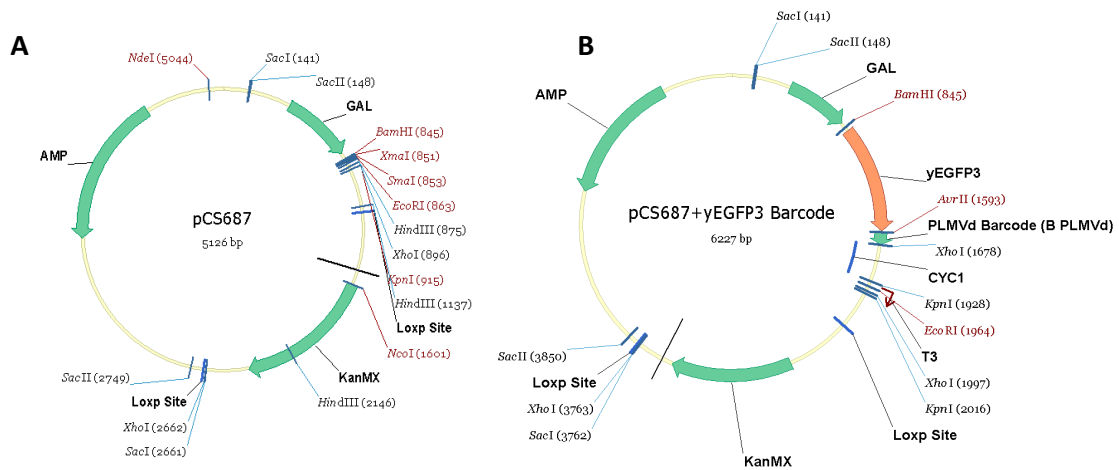
Supplementary Figure 4.11. Plasmid maps for construction of CSY341 expression vectors. A. pCS687. **B.** pCS1340 was constructed from pCS687 adding yEGFP between BamHI and AvrII and B_PLMVd Barcode between AvrII and XhoI.

Supplementary tables

Supplementary Table 4.1. Plasmids

pCS#	Description	Yeast Marker	E.coli Marker
pCS687	LoxP integrating vector, no yeast origin of replication, derived from pCS270, a pUC vector.	KanMX	AMP
pCS1340	pCS687+ yEGFP cloned between BamHI and AvrII and B_PLMVD (5'-) cloned in 3'UTR between AvrII and XhoI	KanMX	AMP
pCS346	Previously constructed by K. Hawkins with two expression cassettes with promoter (pTEF1) and terminator (CYC1t)	URA	AMP
pCS933	pCS346 + tdimer2 between SalI and NotI	URA	AMP
pCS975	pCS933 + cis-cis.STRSV Cassette between SacII and AvrII	URA	AMP
	pCS933 SSCR1 (aka "Rz core mut")	URA	AMP
	pCS933 SSACR (aka "Rz arms mut")	URA	AMP
	pCS933 SS1-(aka "mRz" or "Rz no loops")	URA	AMP
	pCS933 554	URA	AMP
	pCS933 654	URA	AMP
	pCS933 1154	URA	AMP
	pCS933 1154+5	URA	AMP
	pCS933 1654	URA	AMP
	pCS975 SSCR1 (aka "Rz core mut")	URA	AMP
	pCS975 SSACR (aka "Rz arms mut")	URA	AMP
	pCS975 SS1-(aka "mRz" or "Rz no loops")	URA	AMP
	pCS975 554	URA	AMP
	pCS975 654	URA	AMP
	pCS975 1154	URA	AMP
	pCS975 1154+5	URA	AMP
	pCS975 1654	URA	AMP

Supplementary Table 4.2. Ribozyme sequences

Ribozyme	Type	Sequence	Cloning notes
SSCR1	Rz core mut	GGAAAGCATGCTAACAAGTACTGTGAGGTGAAAACCTCCTCACCATGTGGGAGCTCAAAC	Annealed for insert into pCS933; Annealed and SacI and SphI double-digested for insertion into pCS975
SSACR	Rz arms mut	GGAAAGCATGCGATGTCCTGATGAGAGGTGAAAACCTCGAACACGTGAATGAGCTCAAAC	
SS1 (aka mRz)	Rz no loops	GGAAAGCATGCTAACAACTGATGAGAGGTGAAAACCTCGAAACCATGTGGGAGCTCAAAC	
554	Canonical PLMVd Rz	GGAAAGCATGCATTCTTAAAACAACTGATGAGTCGCTGAAATGCGACGAAACCATGTGGGAGCTCAAAC	
654	Canonical PLMVd Rz	GGAAAGCATGCAATTCTTAAAACAACTGATGAGTCGCTGAAATGCGACGAAACCATGTGGGAGCTCAAAC	
1154	Canonical PLMVd Rz	GGTAACAAATTCTTAAAACAACTGATGAGTCGCTGAAATGCGACGAAACCATGTGGC	Annealed for insert into pCS933
1154+5	Canonical PLMVd Rz	GGTAACAAATTCTTAAAACAACTGATGAGTCGCTGAAATGCGACGAAACCATGTGGTCTCTC	
1654	Canonical PLMVd Rz	GGAGCAGTAACAAATTCTTAAAACAACTGATGAGTCGCTGAAATGCGACGAAACCATGTGGC	
1154	Canonical PLMVd Rz	CTAACAAATTCTTAAAACAACTGATGAGTCGCTGAAATGCGACGAAACCATGTGGGAGCT	Annealed for insert into pCS975
1154+5	Canonical PLMVd Rz	CTAACAAATTCTTAAAACAACTGATGAGTCGCTGAAATGCGACGAAACCATGTGGTCTCTGAGCT	
1654	Canonical PLMVd Rz	CAGCAGTAACAAATTCTTAAAACAACTGATGAGTCGCTGAAATGCGACGAAACCATGTGGGAGCT	

Supplementary Table 4.3. Yeast strains

CSY#	Description
132	*MATa his3-11,15 trp1-1 leu2-3 ura3-1 ade2-1, pTEF1-yEGFP-PEST*
341	*MATa his3-11,15 trp1-1 leu2-3 ura3-1 ade2-1, Δgal2, pGAL1-yEGFP*

Supplementary Table 4.4. Cloning primers

Name	Sequence	Notes
tdimer2.K2.fwd	AAAAAAGTCGACATTAAATAATGGTGGCCTCCTCCGAGGA	Sall, NotI restriction sites; PCR of tdimer2 for insert into pCS346
tdimer2.rev	AAAAAAGCGGCCGCGAAATTCGCTTATTTAGAAGT	
Cis-Cis. sTRSV.FWD	GGCTGTCACCGGATGTGCTTTCCGGTCTGATGAGTCCGTGAGGACGAAACAGGCATGCAAAAAGAGCTCCTGTCACCGGATGTGCTTTCCGGTCTGATGAGTCCGTGAGGACGAAACAGC	AvrII and SacII restriction sites; Annealed for insert into pCS933
Cis-Cis. sTRSV.REV	CTAGGCTGTTTCGTCCTCACGGACTCATCAGACCGGAAAGCACATCCGGTGACAGGAGCTCTTTTTGCATGCCTGTTTCGTCCTCACGGACTCATCAGACCGGAAAGCACATCCGGTGACAGCCGC	
tdimer2.SacII.mut.Fwd	CTACAAGGTGAAGTTCAGAGGCACCAACTTCCCCC	Primers to mutate Sac II sites in tdimer2
tdimer2.SacII.mut.Rev	GGGGGAAGTTGGTGCCTCTGAACTTCACCTTGTAG	
GAL2ko.fwd	ATGCACCTTATTCAATTATCATCAAGAATAGTAATAGTTAAGTAAACACAAGATTAACATAATAGTGCGGGCCTCTTCGCTATTACGCCA	Primers amplifying pCS687 for integration of pGAL1-yEGFP into GAL2 locus
GAL2ko.rev:	ATGATAATTAAAATGAAGAAAAAACGTCAGTCATGAAAAATTAAGAGAGATGATGGAGCGTCTCACTTCACTATAGGGAGACCGGCAGAT	

Supplementary Table 4.5. *In vitro* assay primers

Name	Sequence	Notes
T7Rbz 5'-23.FWD	**GAAATTAATACGACTCACTATA**GGCATAGCAATCTAATCTAAGTTTTGC	T7 sequence in bold; 137nt target transcript yEGFP (573-708) 86bp 5' and 51bp 3'
T7Rbz 3'.REV	AATTACATGATGCGGCCCTCTCAACCTA	
Target.yEGFP.FWD	**GAAATTAATACGACTCACTATA**TCCAGTCTTGTTACCAGACAAC	
Target.yEGFP.REV	CAATTCATCCATACCATGGGTAATACC	
137nt target sequence	TCCAGTCTTGTTACCAGACAACCATTACTTATCCACTCAATCTGCCTTATCCAAAGATCCAAACGAAAAGAGAGACCACATGGTCTTGTTAGAATTTGTTACTGCTGCTGGTATTACCCATGGTATGGATGAATTGT	Actual sequence transcribed